Nickel and Iron-Doped Biocarbon Catalysts for Reverse Water-Gas Shift Reaction

Théodore Graul, María González Martínez, Ange Nzihou

▶ **To cite this version:**

Théodore Graul, María González Martínez, Ange Nzihou. Nickel and Iron-Doped Biocarbon Catalysts for Reverse Water-Gas Shift Reaction. ChemCatChem, 2024, 16 (10), 10.1002/cctc.202301398 . hal-04449020

HAL Id: hal-04449020

https://imt-mines-albi.hal.science/hal-04449020v1

Submitted on 22 Feb 2024

HAL is a multi-disciplinary open access archive for the deposit and dissemination of scientific research documents, whether they are published or not. The documents may come from teaching and research institutions in France or abroad, or from public or private research centers.

L'archive ouverte pluridisciplinaire **HAL**, est destinée au dépôt et à la diffusion de documents scientifiques de niveau recherche, publiés ou non, émanant des établissements d'enseignement et de recherche français ou étrangers, des laboratoires publics ou privés.

Nickel and Iron-Doped Biocarbon Catalysts for Reverse Water-Gas Shift Reaction

GRAUL Théodore, GONZÁLEZ MARTÍNEZ María and NZIHOU Ange

Abstract: Biocarbon catalysts for reverse water-gas shift reaction (RWGS) were produced from pyrolyzed fern and willow impregnated with iron and nickel nitrates. This reaction can partake during Fischer-Tropsch synthesis (FTS) by consuming CO_2 and lowering both the H_2/CO ratio and the efficiency in the production of fuels. RWGS has attracted much attention to widespread utilization of CO_2 through the production of syngas. The catalysts were therefore tested in a fixed-bed reactor at 400°C as it is the maximal temperature for FTS and high RWGS. They showed high selectivity towards CO (>84%) and fair conversion (<17%) compared to rust (81%, 30%, respectively) and Fe-impregnated alumina (100%, 8%). No loss in selectivity and conversion was observed for a longer residence time (288h). Biomass inherent metals could provide reactive gas adsorption sites that improve conversion by dispersing electrons which reduces adsorption and dissociation energy barriers. K, Mg and Ca in fern biocarbon catalysts may be related to the higher CO_2 uptake compared to willow catalysts. Electron deficient sites produced by reduction of biocarbon oxygen functional groups may facilitate CO_2 uptake and activation. Ni-impregnated fern-based biocarbon showed the highest activity, due to the synergetic effect of the inherent metals, O vacancies and strong metal-carbon interactions.

Introduction

Greenhouse gas emissions are the main cause of current global warming. This accounts for climate damages including destructive storms, severe droughts and quicker wildfires, among others, which results in an increasing devasting of humanity's livelihood. To limit Earth's warming, the 2015 Paris Agreement engaged the 193 signatory nations to reduce greenhouse gas emissions namely carbon dioxide (CO_2) [1]. Since then, the increase in CO_2 emissions have begun to stagnate in relation to world-wide policies, but also pandemic-related lockdowns and reduced fossil fuel importing. A rebound resulting in an increase of these emissions is therefore expected for the upcoming years [2–4]. Consumption of CO_2 via chemical (ex. thermal conversion) or biologic pathways (ex. photosynthesis) or restriction of its production by optimizing CO_2 producing processes are means to limit its emission. Therefore, biomass and biowaste valorization into hydrogen (H_2), biofuels and other products may play a significant role in reaching this objective, due to the carbon neutrality and high availability of these bioresources [2].

Thermochemical conversion processes of bioresources to produce syngas, containing H_2, tar and biocarbon (understood as biochar) typically require high temperatures (between 500 to 1000°C) and the use of catalysts allows lower operating temperatures and energy saving. Fischer-Tropsch synthesis (FTS) however allows the production of synthetic fuel from synthetic gas composed of mainly carbon monoxide (CO) and H_2 at milder conditions. This process, operating from 180 to 400°C and around 20 bar, requires noble or transition metal-based catalysts, including iron (Fe) and nickel (Ni) [5,6]. It also performs best under H_2/CO of 2 [7]. Therefore, reverse Water-Gas Shift (RWGS) is effective for integration with FTS reactions by reversibly converting CO_2 and H_2 into CO and H_2O. This will translate into a CO_2 consumption to produce synthetic fuels and reduce H_2/CO in syngas for use in FTS (**Eq.**1) [8]. This reaction requires similar catalysts to those of FTS and higher temperatures due to its endothermicity ($\Delta H^0_{298} = 42.1\ kJ/mol$) but can be performed simultaneously to FTS by reducing the temperature (to 400°C) [9].

$$CO_2 + H_2 \leftrightarrow CO + H_2O \qquad \textbf{Eq.}1$$

Fe has catalytic activity for RWGS and is generally promoted by alkaline and alkaline-earth metals (AAEM) namely K, Mg and Na, or Ni, Cu and Co [10–13]. Fe promoted by Cu can reach CO_2 conversion as high as 45% at 400°C with close to 100% RWGS selectivity [12]. Fe allows strong CO_2 adsorption through strong electron exchange and O vacancies that accept CO_2 electrons (Lewis base). Fe and Ni can be supported by Al_2O_3, SiO_2, CrO_2. These supports and the promoters prevent sintering, coking and other deactivation phenomena, through transformation of the active phase, while improving reactant adsorption thanks to O vacancies. These promoters and supports can also adjust selectivity towards a specific product, CO for RWGS, by weak adsorption and fast removal because of limited electron availability [9,10,14–17]. Ni favors CO and CH_4 formation so promotion and support can be necessary for its selectivity [9,18–20]. Ni promoted by Cu can reach conversion as high as 50% at 400°C but at the cost of decreasing selectivity to at most 75% [20]. Fast CO desorption with low H_2 adsorption could also unlock access to active sites for CO_2, increasing catalytic performance. Promoters can help reducing the energy necessary for adsorption and desorption in addition to providing further adsorption sites [9,15–17]. Biocarbon can act as a potent support allowing strong metal-surface interaction and increased O vacancies related to the bond between metal and carbon that furthers electron transfer, and the

reduction of O functional groups respectively [21,22]. The dispersion of the metal active sites and the adsorption of gases are also affected because of this bond and are linked to the porous structure of biocarbon (site availability) and heterogenous surface sites (different electron density) [23,24]. Other transition metals such as Cu are also active for RWGS with high selectivity (nearly 100%) and activities that could reach 35% at 550°C [25]. Noble metals such as Pt supported on CeO_2 can reach 45% conversion at 450°C with more than 97% selectivity [26]. Au on TiO_2 can achieve 40% conversion at 450°C with high selectivity [27]. Fe and Ni were studied as lesser toxic and more available metals [28–30].
Metallic catalysts have a high environmental impact because of the metal extraction processes that are energetic and intensive in solvent, and are highly scarce [17,31,32]. These metals can be sourced more sustainably through plant phytoextraction and could then be transformed into catalysts [33,34]. This transformation can be achieved through pyrogasification. The high temperature (>500°C) could form ordered carbon structures with interesting properties such as increased surface basicity that in the case of RWGS could allow improved CO_2 adsorption and further reaction. It could however also inhibit availability of active metal sites as they could sinter [35,36]. Low heating rates (<50°C/min) could assist micropore formation that expose active sites, and prevent alkaline metal volatilization that promote RWGS active sites. Smaller pores are however easily blocked [17,36–38]. Fixed and fluidized bed are the most common reactors for this transformation as the transformation is facilitated in relation to the compacity of this bed. This could raise issues concerning heat and mass transfer limitations [39]. Pore development could be facilitated under H_2O or CO_2, but for a catalytic application, the improved catalytic metal retention provided under N_2 is necessary [37,38,40].
To overcome the burden that metallic catalysts face, in this work, we aim at producing and characterizing innovative catalysts from pyrolyzed metal-loaded bioresources and test them in RWGS.

Materials and methods

Preparation and utilization of the biocarbon catalysts

Fern and willow were selected as raw bioresources because of their ability to cumulate heavy metals from soil in phytoremediation. Willow was harvested in the South of France in 2015. Fern corresponds to shrublands mainly composed of fern harvested in Brittany (France) in 2019.
To mimic heavy metal content in phytoremediation and to obtain a biocarbon catalyst with a controlled metal content, both biomass and resulting biocarbon were impregnated. A 98 wt% pure Ni nitrate ($Ni(NO_3)_2{\cdot}6H_2O$) and Fe nitrate ($Fe(NO_3)_3{\cdot}9H_2O$) solutions containing traces of other metal elements including Co, Cu, Zn and Si, were used for this aim. For biocarbon catalysts preparation, biomass was pyrolyzed under 1L/min nitrogen (N_2) from 25°C to 800°C, at 2°C/min, followed by an isothermal step at 800°C for an hour.
In a second step, impregnation was carried out to reach a metal load of 30mg per kg of biocarbon. Wetness impregnation (WI) was applied to biomass: 20g of biomass was submerged in different 1L aqueous solutions containing Fe or Ni nitrates, stirred for 3 days and then dried for 1 day at 60°C [32]. WI based on insipient WI (IWI) was applied to biocarbon: wettable volume and amount of nitrate to attain a fixed percentage of metal in biocarbon helped determine a concentration of nitrate to thereafter be replicated in 100mL of water for 2g of biocarbon [6]. The solutions were stirred for varying amounts and time and then dried for 1 day at 60-105°C. Unimpregnated fern (RF) and willow biocarbon (RW) were prepared in the same conditions of pyrolysis for comparison. 500°C stability was observed under 24-hour exposure to N_2 at 500°C by following mass loss (4wt% for the 24h on average for all biocarbon catalysts).

Biocarbon catalysts were then tested for RWGS reaction in a fixed bed reactor (Top Industries (France), 8 mm diameter, 25 cm long, **Figure 1**). The reactor was filled with the catalyst and an inert bed of alumina (θ-Al_2O_3, [41]), which steadied the catalysts position in the isothermal area of the reactor [5,6]. Moisture was removed before reaction by flowing Ar at 120°C for 1h and samples were then pre-reduced under 60/40 vol% H_2/Ar at 500°C for 2h. RWGS was carried out at 400°C, for at least 3 bars during a maximum of 72h. Gas flows used were 60 mL/min of H_2, 20 mL/min of CO_2, and 150 mL/min of Ar. All gases were preheated at 120°C before being introduced in the reactor. Dried permanent gases (CO, CO_2, H_2, CH_4) were analyzed by online µ-GC/TCD (Agilent 990) connected after the reactor [9].
To compare experimental results, equilibrium of RWGS was calculated only considering the species involved in the reaction at the conditions of the reaction. These conditions were 400°C and initially 20 mL/min CO_2 and 60 mL/min H_2. Equilibrium values were determined using the expression of equilibrium constant according to concentrations of reactive and produced gases at equilibrium, and reported values for the WGS equilibrium constant (**Eq**.2, $K_{eq,WGS}$ = 11.74) [42].

$$K_{eq,RWGS} = \frac{[CO]_{eq}[H_2O]_{eq}}{[CO_2]_{eq}[H_2]_{eq}} = \frac{1}{K_{eq,WGS}} \qquad \textbf{Eq}.2$$

Following these calculations, the flow rates at equilibrium of the reactive and produced gases are 52.94 mL/min of H_2, 12.94 mL/min of CO_2, 7.06 mL/min of CO and 7.06 mL/min of H_2O. Ar flow rate remains unchanged. This results in a conversion rate of CO_2 to CO of 35% at equilibrium.

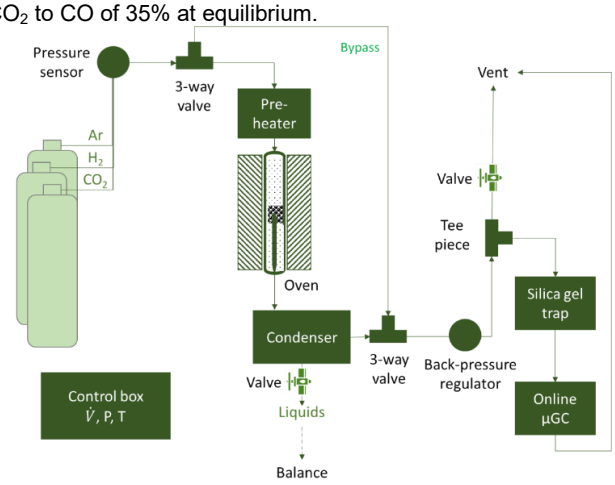

Figure 1. Set-up for the Reverse Water-Gas Shift (RGWS) experiments

Biocarbon catalysts were characterized in terms of inorganic elements content by inductively coupled plasma atomic emission spectroscopy (ICP-AES, Ultima 2) and their dispersion on the carbonaceous matrix by high resolution transmission electron microscopy (HRTEM, JEOL JEM-ARM200F), surface area by N_2 adsorption isotherm using Brunauer-Emmett-Teller method (BET, N_2, Tristar II 3020 and 3Flex), textural properties and surface chemical groups by temperature programmed desorption, reduction and oxidation and by X-ray diffraction (TPD, TPR, TPO, Micromeritics Autochem 2920; XRD, PANalytical X'PERT PRO MDP). The changes in the structure of the biocarbon catalyst were analyzed before and after the chemical reaction.

Performance of the biocarbon catalysts

The performance of the biocarbon catalysts was evaluated by the mean of selectivity and conversion rate. Selectivity (S) allows to compare produced molecules and identify, in this case, if CO_2 forms preferentially CO or CH_4. Therefore, selectivity was defined as the ratio of the molar or volumetric flow ($\dot{V}$) of the target carbon gases produced compared to the sum of all carbon gases produced through the reaction (**Eq**.3 and 4).

$$S_{CO} = \frac{\dot{V}_{CO}}{\dot{V}_{CO}+\dot{V}_{CH4}} \quad \textbf{Eq.}3$$

$$S_{CH_4} = 1 - S_{CO} \quad \textbf{Eq}.4$$

Conversion rate of the limiting gas CO_2 represents consumption of this gas to form products. A higher conversion represents a higher activity from the biocarbon catalyst. Conversion (X) was therefore defined as the ratio between the consumed amount of CO_2, calculated by the difference of inlet and outlet flowrate, divided by the inlet flow rate of the respective gas (**Eq.**5).

$$X_{CO_2} = \frac{\dot{V}_{inlet,CO_2} - \dot{V}_{outlet,CO_2}}{\dot{V}_{inlet,CO_2}} \quad \textbf{Eq.}5$$

Results and Discussion

Performance of biocarbon catalysts on RWGS

The performance of the catalysts was evaluated through CO selectivity and CO_2 conversion comparing type of bioresource (fern and willow, F/W), type of impregnation (before and after pyrolysis, B/A), and type of metal impregnated (Fe and Ni). The results present little variation during the experiment. They are therefore summarized in terms of the concentration of the reactive (H_2 and CO_2) and the product gases (CO and CH_4), the selectivity towards CO and CH_4 and the CO_2 conversion. This allows the comparison of the catalytic activity between biocarbon catalysts, reference catalysts and equilibrium conditions (**Table 1**). The pre-reduction step was compared to the not pre-reduced fern biocarbon impregnated after pyrolysis with Ni (FNi-A no red.). Long use of biocarbon catalyst was tested using fern biocarbon impregnated before pyrolysis with Fe (FFe-B long). Rust (Fe_2O_3) and Fe-doped alumina (Fe-Al_2O_3) were tested for comparison [15,43].

Table 1. Summary of averaged concentrations, selectivity and conversion for the trialed catalysts.

Operating conditions: 400°C, H_2/CO_2 = 3, 72h on stream (24h for rust and 288h for long)					Concentration of gases (vol%)				Conversion	Selectivity (%)	
					H_2	CO_2	CO	CH_4	X_{CO_2} (%)	S_{CO}	S_{CH_4}
Biocarbon (BC) and reference catalysts				Initial composition	26.1	8.7	-	-	-	-	-
				RWGS equilibrium	23.0	5.6	3.1	-	35.0	100	0
Sample	Biomass	Metal	Metal content (wt% BC)	Impregnation before/ after pyrolysis	Concentration of gases (vol%)				Conversion	Selectivity (%)	
					H_2	CO_2	CO	CH_4	X_{CO_2} (%)	S_{CO}	S_{CH_4}
RW	willow	-	-	-	21.9	7.4	0.1	<0.0	9.1	100	0
WNi-B	willow	Ni	2.41	before	21.7	7.5	0.1	<0.0	8.0	99.4	0.6
WNi-A	willow	Ni	1.81	after	21.8	7.5	0.2	<0.0	8.8	97.4	2.6
WFe-B	willow	Fe	4.64	before	21.8	7.2	0.2	<0.0	9.2	98.2	1.8
WFe-A	willow	Fe	0.23	after	21.9	7.5	0.1	<0.0	5.7	100	0
RF	fern	-	-	-	21.9	7.4	0.1	<0.0	10.0	100	0
FNi-B	fern	Ni	3.96	before	21.8	7.4	0.2	<0.0	8.5	97.8	2.2
FNi-A	fern	Ni	1.43	after	21.2	6.7	0.8	0.1	15.5	88.3	11.7
FFe-B	fern	Fe	13.17	before	21.1	6.8	0.9	<0.0	16.1	98.0	2.0
FFe-A	fern	Fe	0.51	after	21.8	7.5	0.1	<0.0	5.0	100	0
FNiFe	fern	Fe,Ni	10.30, 8.08	before	21.1	6.9	0.6	<0.0	14.3	96.7	3.3
FNi-A no red.	fern	Ni	1.43	after	21.0	6.7	0.9	0.1	17.2	94.4	5.6
FFe-B long	fern	Fe	13.17	before	21.0	6.7	0.9	<0.0	17.1	97.5	2.5
Rust	-	Fe	-	-	18.9	5.5	1.8	0.4	29.6	81.0	19.0
Fe doped alumina	-	Fe	-	-	21.5	7.3	0.3	<0.0	7.6	100	0

Values for CO (and other gases) concentration are in a comparable range to equilibrium concentration (3.1 vol%, **Table 1**). The values may appear as low, due to the Ar dilution, but remain above µGC detection limit (0.001 vol%). The most active biocarbon catalysts were tested twice, the maximum relative standard deviation obtained was 5.5%.

The catalysts present a high selectivity towards CO, which is reflected by the low CH_4 production. This is especially relevant compared to the rust (88-100% versus 81%), which is usually taken as a reference. It should be noted that selectivity towards CO is high (>80%) for all catalysts and in these operating conditions despite the fact that CH_4 is formed thermodynamically [9,44,45]. Reported metallic catalysts can reach selectivity close to 100% but the promoting effect of other metals, such as K, is necessary [10,16]. Some biocarbon catalysts showed conversion rates lower than that of Fe-doped alumina, while others are more performant (at most 17.2% compared to 7.6%). Their performance is however inferior to rust (29.6%) or other reported catalysts (near equilibrium, in this case 35%) [46]. On another hand, the performance of the biocarbon catalysts was stable as no loss in conversion was observed during 288h on stream. In contrast, metallic catalysts are deactivated by sintering and C fouling before 120h (24h for the rust studied here) [10,16,17].

The type of bioresource proved to have an effect on RWGS, as fern catalysts showed a higher CO_2 conversion at the cost of CO selectivity (**Table 1**). This behavior may be explained by the higher inherent metal content in fern, obtained through ICP-AES analysis (**Table 2**). According to the elemental composition for unimpregnated biocarbon, total inorganic content and composition are coherent with reported fern and willow. Slight differences observed could be due to the origin of the biomass (soil, species, age, …) [47–52]. Impregnated biocarbon content is higher than that reported for phytoremediation and hyperaccumulation plants to clearly show the effect of Ni and Fe as catalysts in RWGS [53–59]. Nevertheless, it can be noted that AAEM were leached due to impregnation but Ni or Fe content increased and could be comparable to thresholds for hyperaccumulation (3000 µg/g biocarbon, [59]). The content of some heavy metals such as Zn could increase with impregnation due to their introduction in the impregnation medium as impurities of the Fe and Ni nitrates.

The results showed that fern-based biocarbon converts better the reactive gases of RWGS (**Table 1**). This difference in performance compared to the willow biocarbon could be firstly explained by inorganic elements (**Table 2**). AAEM in fern biocarbon could facilitate reducibility and stability of active metals by lowering energy barriers and preventing their transformation and sintering. The synergy of these metals could limit the uptake of H_2 therefore preventing hydrogenation of CO, in addition to allotting more sites for an increased CO production [60–63]. They can also result in higher CO_2 reactivity and better activation from fern biocarbon catalysts. This could be explained by a better electronic transfer and an increase in reactive sites.

Table 2. Inorganic composition (µg/g biocarbon) of willow and fern biocarbon catalysts before RWGS

	RW	WNi-B	WNi-A	WFe-B	WFe-A	RF	FNi-B	FNi-A	FFe-B	FFe-A	FNiFe
Na	245	<1	<1	<1	<1	3822	<1	<1	1218	<1	904
K	6660	2003	1860	1395	1859	19192	5134	4565	3976	6588	3619
Mg	1968	745	1455	562	1049	2759	904	380	887	720	1055
Ca	23393	7349	7117	1059	6862	9321	4446	7818	3436	8110	4708
Mn	172	<1	<1	74	<1	68	<1	<1	73	<1	186
Fe	279	<1	<1	46409	2276	263	<1	<1	131669	5098	103030
Co	186	<1	<1	51	<1	245	<1	31	311	<1	750
Ni	16	24075	18147	45	<1	1	39580	14282	49	<1	80800
Cu	<1	<1	<1	82	<1	<1	<1	<1	<1	<1	1
Al	81	456	489	127	3481	172	742	<1	2877	43	1448
Zn	67	846	819	<1	822	19	927	<1	21	<1	311
Cd	<1	<1	<1	21	<1	<1	<1	<1	<1	<1	1
Si	1058	401	1327	<1	2197	17450	14040	20870	44151	31987	45653
P	3607	<1	2489	<1	300	2257	1500	1207	3989	1203	4473

The multitude of fern biocarbon (RF) inherent metals was also observable by HRTEM (**Figure 2**). Some elements such as Mg, K and Cl are highly dispersed on the carbon surface, others such as Ca and Si are more agglomerated with a particle size reaching 27nm. Similarly, dispersed O, which indicates O groups related to the carbon surface or O containing metal speciation, seems denser in areas were Si and Ca are located. These results are in agreement with XRD characterizations (**Figure 3**), which show that Si is in an oxidized state. However, these metals seem covered by a carbon layer without a structured morphology, meaning that the active sites might not be accessible for RWGS activity.

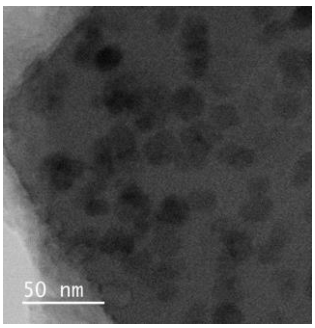

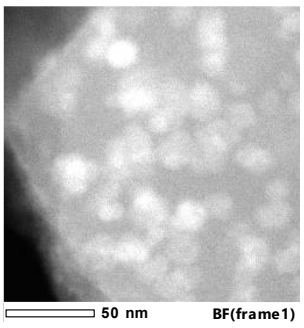

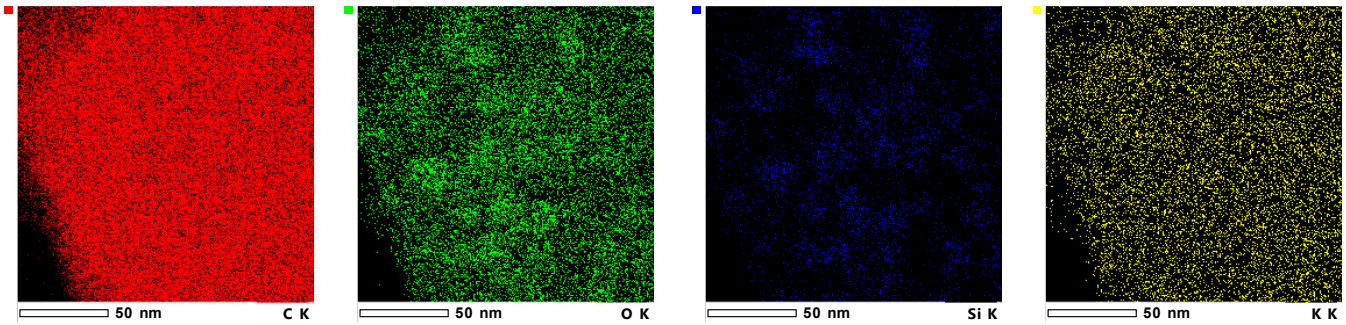

Figure 2. HRTEM images of unimpregnated fern biocarbon (RF) before its use in RWGS

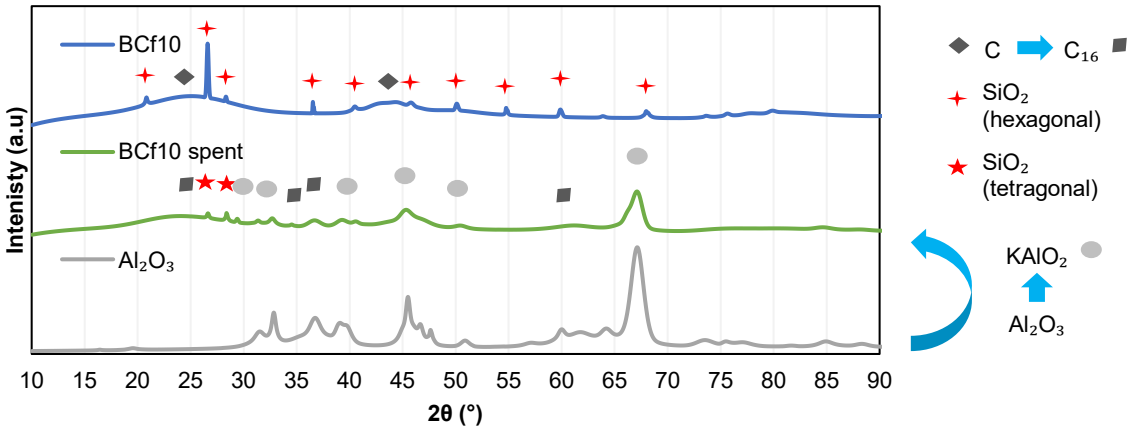

Figure 3. XRD diffractogram of unimpregnated fern biocarbon not spent and spent by RWGS (and Al_2O_3)

The high activity of FNi-A could be linked to dispersion of Ni. Varying sizes of particles were observed, reaching hundreds of nanometers. They could possibly be in an oxidized state before reaction that once reduced results in O deprived sites that could facilitate the capture of O from CO_2 (**Figure 4**). As Ni was deposited on the surface of the biocarbon, it is possible that they were easily accessible, which may explain the enhanced activity of this catalyst.

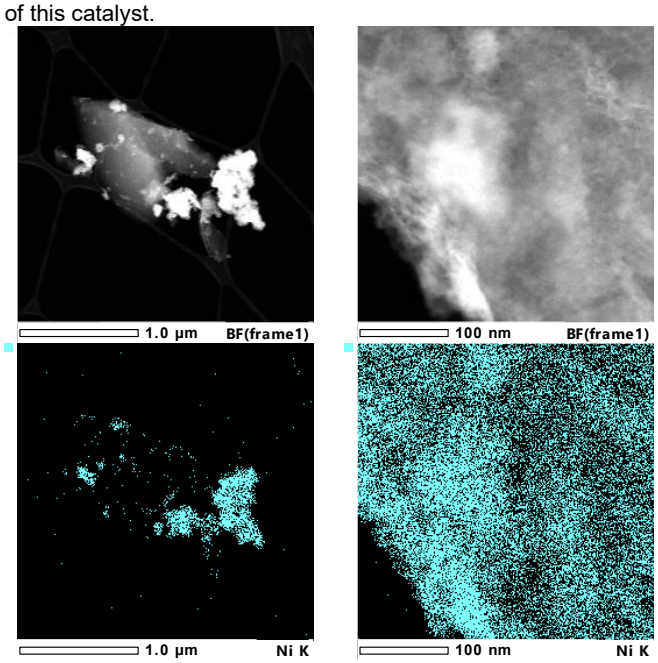

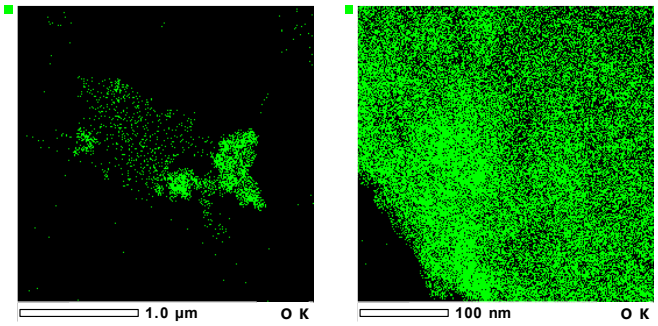

Figure 4. HRTEM images of fern biocarbon impregnated with Ni after pyrolysis (FNi-A) before its use in RWGS

This variety in particle size also stands out with fern biocarbon impregnated with Fe before pyrolysis (FFe-B), as big as 56 nm, and in a possible oxidized state (**Figure 5**). The addition of Fe could however create an ordered state of carbon (graphitization) and an external shell composed of Fe and C surrounding an Fe dense structure [64,65]. This could induce an increase in specific surface area, and improve electric and thermal conductivity which are favorable for O and CO_2 transport [66].

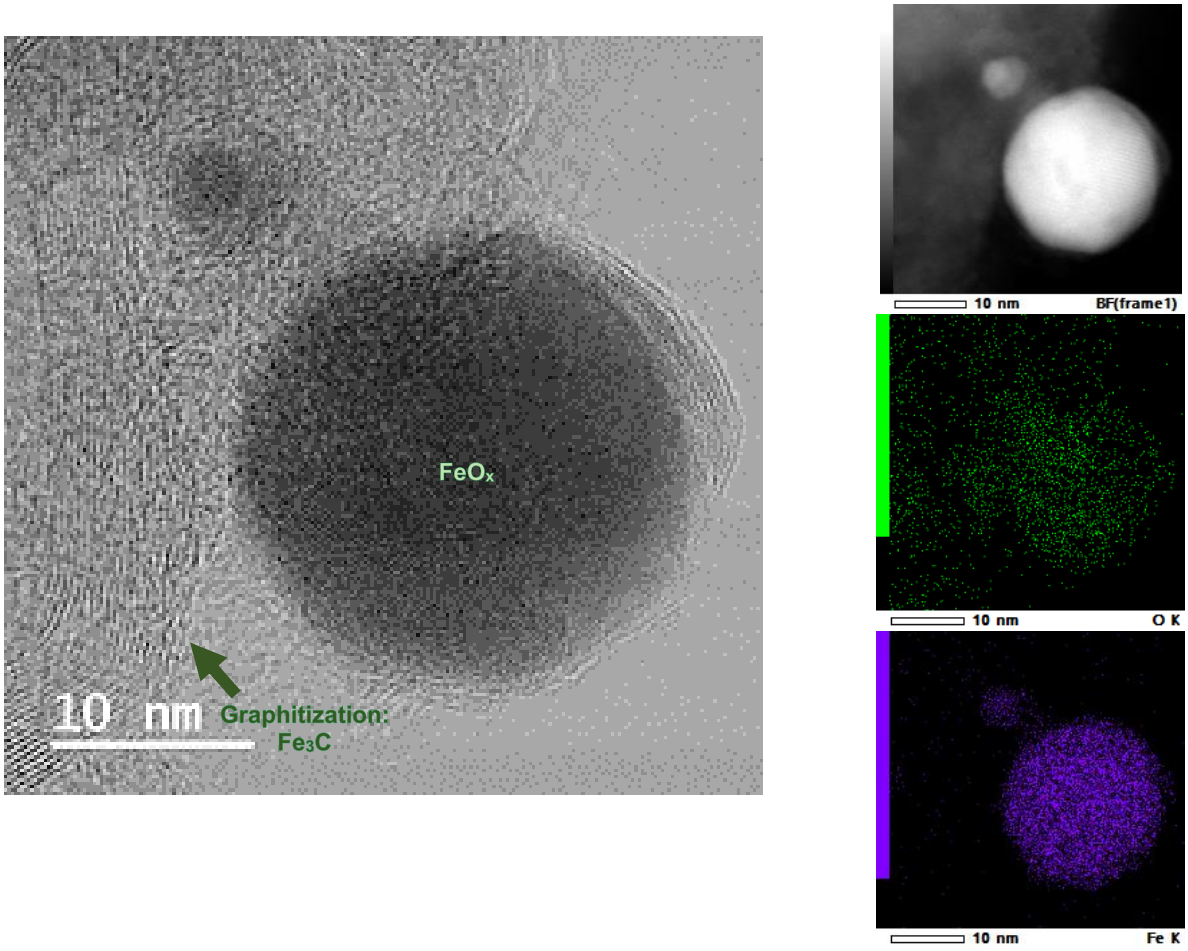

Figure 5. HRTEM images of fern biocarbon impregnated with Fe before pyrolysis (FFe-B) before its use in RWGS

The type (acid, basic, reduction sites) and force (value of maximal temperature) of surface chemical functions were measured through temperature programmed desorption (TPD, NH_3), oxidation (TPO, CO_2) and reduction (TPR, H_2, **Table 3**). The total amount of adsorbed probe gases, corresponding to the sum of the area of peaks from TPX (X = D, O, R), and the specific surface area, obtained via BET measurements under N_2, were indicated (**Table 3**).

The values for the total quantity of adsorbed NH_3, CO_2, H_2 and the specific surface area were found to be inferior for fern-based biocarbon catalysts than for willow-based. This contrasts to the higher metal content of fern biocarbon catalysts. Therefore, fern-based biocarbon should possess a higher and stronger surface basicity in relation to this higher metal content. This would enable more CO_2 adsorption and higher desorption temperature. Given the adsorptive nature of the unimpregnated biocarbon, surface functional groups could be responsible for a higher and stronger uptake of gases compared to the metals [67–69]. This could explain why willow-based biocarbon having better gas adsorptive properties does not result in better RWGS performance as it lacks the synergetic effect provided by other metals (**Table 2**). Lower specific surface area could be due to lower volatile matter content resulting in less porosity formed during pyrolysis, which is coherent with the literature results for herbaceous biomass such as fern [49,70]. Impregnation seems to impact little the chemical adsorption. This could be explained by the impregnation of metals Fe or Ni on the biomass or biocarbon compensated by AAEM leached by the impregnating medium. Additionally, a decrease in adsorption is possible if the impregnating metals block porosity and should result in an equal loss of specific surface area. In this case, the specific surface area increases with impregnation. In the case of impregnation before pyrolysis, this increase could be related to the development of pores during catalyzed pyrolysis or due to opening of enclosed pores during impregnation after pyrolysis [71,72]. In certain cases, it is possible that the presence of Fe in the initial biomass favors the graphitization of carbon, as it was evidenced by HRTEM (**Figure 5**). This creates porosity, which could explain the high specific surface for these catalysts. According to the results, the specific surface area seems decorrelated from the gas adsorption. There is a slight effect of pore blocking or opening that could affect specific surface area but does not impact the availability of the functional groups. This could be again related to the biocarbon functional groups being responsible for the gas adsorption and therefore a modification in surface area barely modifies the gas adsorption because of the omnipresence of the functional groups. This however affects the activity of the catalysts as a severe loss in surface area (a collapse of porosity) induces a loss in availability of active sites and in turn results in (Fe) doped biocarbon catalysts even lesser active than undoped ones (**Table 1**).

Table 3. Chemical surface groups versus specific surface area of the biocarbon catalysts, before RWGS, and after for specific surface area (72h time on stream)

Sample	TPD-NH_3		TPD-CO_2		TPD-H_2		Specific surface area (m^2/g)	
	Total adsorption (mmol/g)	T_{max} (°C)	Total adsorption (mmol/g)	T_{max} (°C)	Total adsorption (mmol/g)	T_{max} (°C)	Raw	Spent
RW	1.460	889	23.288	907	1.501	999	42.4	115.3
WNi-B	1.968	949	25.458	914	0.282	988	419.1	215.9
WNi-A	1.548	930	26.260	915	2.922	986	336.4	158.1
WFe-B	1.249	960	27.773	935	2.108	985	384.2	145.8
WFe-A	1.255	940	14.810	960	1.393	982	9.2	183.8
RF	0.779	913	12.003	915	2.545	993	8.8	50.8
FNi-B	1.480	912	16.207	920	2.921	986	151.6	186.2
FNi-A	0.847	945	11.956	923	1.673	989	100.0	140.3
FFe-B	0.553	951	8.258	905	0.158	981	309.6	148.5
FFe-A	0.840	951	10.918	956	2.617	981	27.4	169.1
FNiFe	1.088	923	15.980	924	0.994	1000	367.9	237.1

In the case of willow biocarbon catalysts, the catalytic activity seems independent to the impregnation method (before or after pyrolysis) or the metal (Fe or Ni, **Table 1**). Stronger differences could be observed for fern biocarbon catalysts (**Table 1**) and the best results were obtained for fern biocarbon impregnated with Fe before pyrolysis (FFe-B), impregnated with Ni after pyrolysis (FNi-A) and impregnated with Fe and Ni before pyrolysis (FNiFe). This could be related to the high dispersion of highly active sites of small particle size in combination with inherent metals (ex. K) and O vacancies that could be observed by HRTEM (**Figures 2 and 4**). They enhance reactivity and facilitate adsorption and transformation of CO_2 and H_2 [73–75].

The nature of the O surface functional groups of biocarbon catalysts can be evidenced by TPD coupled with µGC. An inert gas (He) is used to transport gases produced and desorbed by the biocarbon. This analysis provides insights on the type of functional group knowing the desorbed gases released (CO or CO_2 here) by the surface of the adsorbent and the temperature at which they desorbed [68,76–78]. Deconvoluting the peaks detected in µGC using Gauss equations can inform about the type of site. By correlating the temperature of desorption and the desorbed gas with data from literature, it is possible to identify and quantify the functional group. Once reduced, these O functional groups create O vacancies which are involved in electron transfer in RWGS.

In the case of fern biocarbon impregnated with Fe and Ni before pyrolysis (FNiFe), only CO_2 was released (**Figure 6**). By deconvoluting the CO_2 production of this catalyst before its use in RWGS (**Figure 6**, top), the 4 Gauss curves were attributed to carboxylic (200 to 430°C) and lactone (190 to 900°C) functions of increasing strengths (higher peak temperatures). While carboxylic groups are amphoteric, lactone groups are strictly basic. This contradicts the fact that biocarbon adsorbed more CO_2 than NH_3 without reduction (**Table 3**), as CO_2 is also basic. When reduced, these functional groups were deprived of O and will attract O containing species such as CO_2. Since here the RWGS reaction involved a step of pre-reduction and exposure to H_2, the lack of O surface functions after reaction was expected as no CO was produced and very little CO_2 (**Figure 6**, bottom). The presence of these groups and that of inherent metals in the biomass allows a better activation and adsorption of the reactants due to stronger electronic properties. This also facilitates the desorption of the products and a better H spillover, which helps in separating H_2 and CO_2 in order to form H_2O and CO [74,79,80].

An exact trend regarding the spent catalysts specific surface area could not be determined (**Table 3**). The values seem to uniformize, increasing when the raw catalyst had little specific surface area (RF) or decreasing when high (WNi-B). This may be related to the addition of alumina (81.7 m^2/g) that could not be separated after reaction.

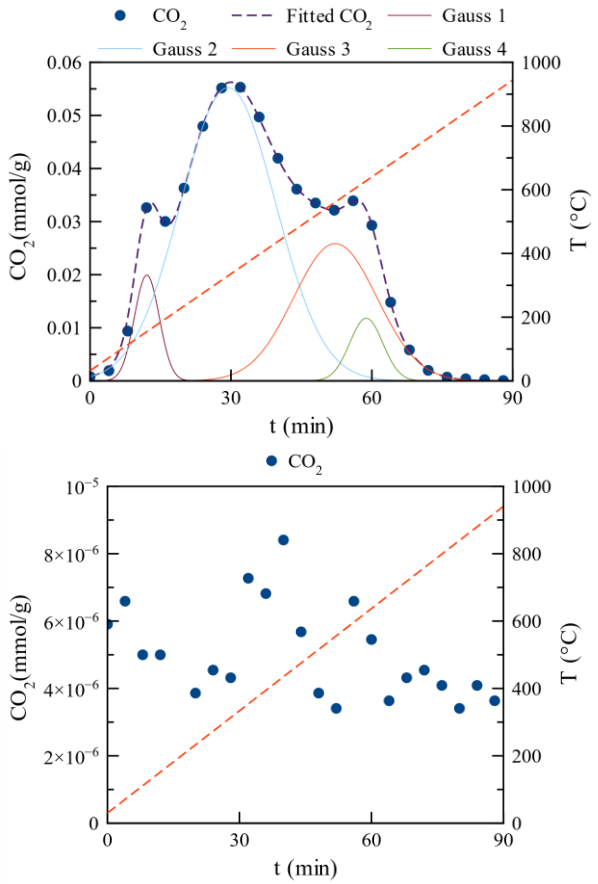

Figure 6. CO_2 desorbed while increasing temperature of FNiFe before RWGS (top) and after RWGS (bottom)

The presence of iron carbides (Fe_3C) in FFe-B was detected by XRD, and could be related to the biocarbon graphitization (**Figure 5**). Fe_3C contributes to improved H_2 and CO_2 activation and dissociation due to the difference in electronegativity, in relation to the developed thermal and electric conductivities, facilitating the acceptance of electrons by Fe (**Figure 7**) [11,44,81]. The alumina mixed with the biocarbon catalyst is also functionalized by reaction with the K naturally present in fern (**Figures 7 and 8**). By attrition, fern-based biocarbon loses K on its surface, diminishing the potential additional CO_2 adsorption and reaction related to its synergy with Fe active sites [77]. It should also be noted the difficulty to reduce this alumina as it conserves an oxidized state and should therefore contribute little to the RWGS reaction that involves a change of state [46].

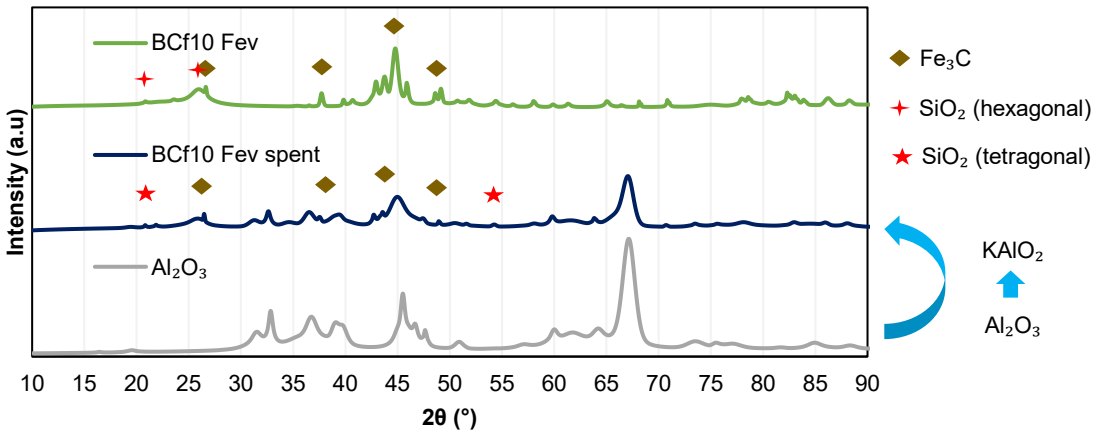

Figure 7. XRD diffractogram of fern biocarbon impregnated with Fe before pyrolysis spent and unspent by RWGS (and Al_2O_3)

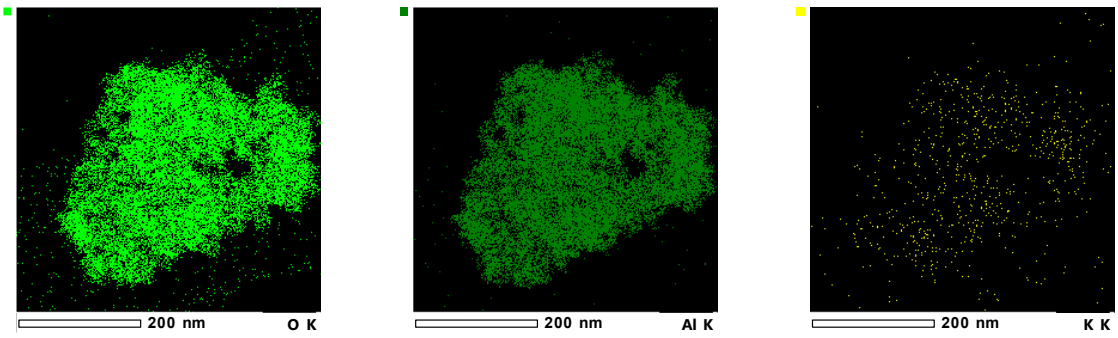

Figure 8. HRTEM images of alumina after RWGS with RF, loss of metals on alumina

Comparison with metallic catalysts and change in conditions

Rust and Fe-doped alumina were tested under the same conditions as the biocarbon catalysts (**Figure 9**). CO_2 conversion and CO selectivity were unstable during the 24h on stream of rust. Furthermore, the effect of the duration of the experiment was investigated by testing the fern catalyst impregnated with Fe before pyrolysis (FFe-B long) during 288 hours (**Figure 9 and 10**). Finally, the effect of the reduction was assessed through the use of the fern catalyst impregnated with Ni after pyrolysis (FNi-A no red) without reduction before reaction.

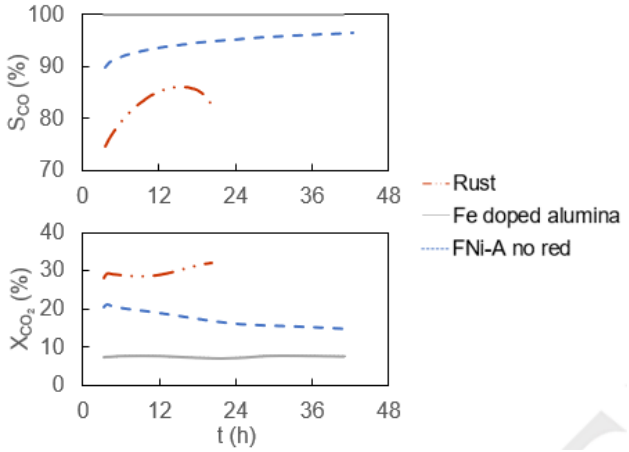

Figure 9. Selectivity in CO (top) and conversion of CO_2 (bottom) of reference and biocarbon catalysts tested in RWGS at 400°C, with test of the effect of reduction on the biocarbon catalysts

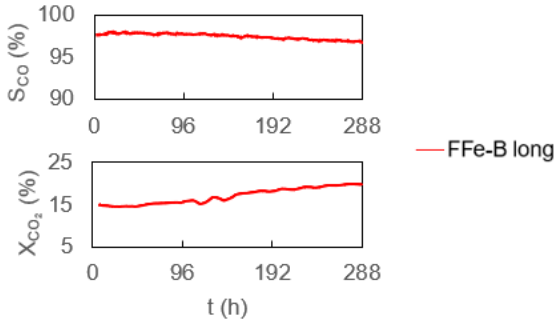

Figure 10. Selectivity in CO (top) and conversion of CO_2 (bottom) of biocarbon catalyst tested in RWGS at 400°C with test of the effect of the duration

The catalytic activity of rust decreased with the production of CO, but then increased with the increasing production of CH_4. This first step of deactivation has been reported and attributed to the formation of Fe carbides [10,82]. During the experiment, the rust captured C up to 9.45 wt%. The presence of C and reducing atmosphere such as H_2 render the formation of Fe_3C possible (**Figure 11**) and, despite being an active phase, its formation in-situ induces loss of active sites by preventing access to the reacting gases [16,81]. This could explain the higher presence of C and the shell-like structure of Fe observed in HRTEM of rust after RWGS (**Figure 12**). This Fe ends up encapsulated by lowly structured C, that could result in the formation of Fe_3C, so Fe becomes unavailable for reaction.

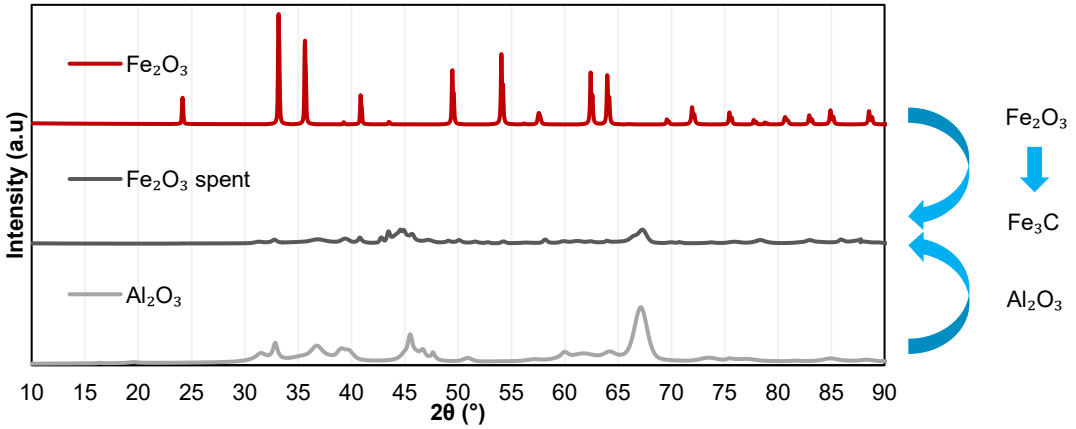

Figure 11. XRD diffractogram of rust not spent and spent by RWGS (and Al_2O_3)

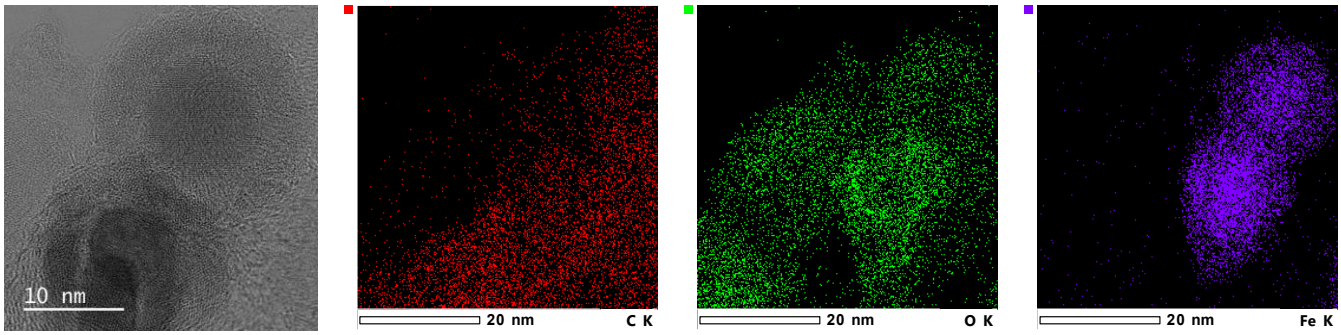

Figure 12. HRTEM images of rust after RWGS

FNi-A was one of the best biocarbon catalysts in RWGS experiments and could have been in an oxidized state before RWGS (**Figure 4**) compared to FFe-B that was in a partially reduced state (**Figures 5 and 7**). The oxidized state of Ni was however not evidenced by XRD as no peaks related to Ni were identified (**Figure 13**), possibly due to low crystalline content of Ni in the biocarbon that is inherently rich in other metals, namely Si, and further diluted by the presence of alumina after RWGS. The use of FNi-A without pre-reduction resulted in slightly better conversion and selectivity. This behavior may be due to a slight agglomeration of Ni° when the catalyst is pre-reduced [23,83–85]. Likewise, the catalyst not having adsorbed H_2 is favorable to immediately adsorb and dissociate CO_2, whose adsorption is more important than that of H_2 (**Table 3**). It can also simultaneously adsorb lesser amounts of H_2 that are then dissociated to react with adsorbed CO_2 according to reported mechanisms [86]. Lesser H_2 adsorption may also prevent further hydrogenation that form CH_4 [73,86,87].

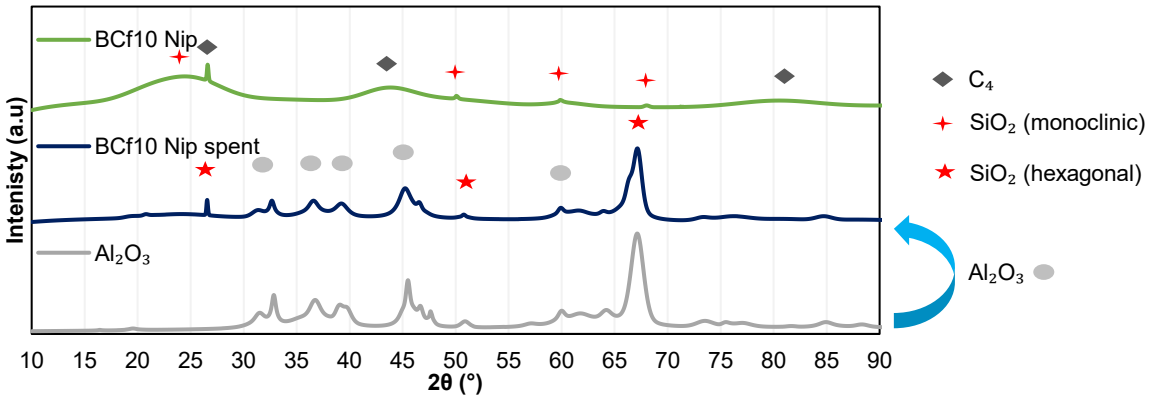

Figure 13. XRD diffractogram of fern biocarbon impregnated with Ni after pyrolysis not spent and spent by RWGS (and Al_2O_3)

Fern biocarbon impregnated with Fe before pyrolysis was tested for 288h (FFe-B long) to investigate Fe deactivation. The biocarbon catalyst resulted in better conversion with little impact on selectivity. Fe catalysts can be deactivated via high temperature sintering or fouling by C deposition resulting also in loss of active sites [9,14,17,81]. In this case, no loss in activity was observed because of the presence of the active Fe_3C phase that, together with the mild operating conditions, may prevent meaningful sintering (**Figure 10**). Indeed, no significant difference in particle size was observed (less than 56 nm), and the slight constant increase in conversion observed over time could be related to better accessibility of the metals as the biocarbon is further graphitized by Fe (**Figure 14**). This could be related to an increase in specific surface area from 148.5 (spent, Table 3) to 188.5 m²/g (288h). NH_3 and CO_2-TPD for FFe-B long showed less gas adsorption capabilities, 0.333 and 4.393 mmol/g, than its raw counterpart (**Table 3**). This indicates a loss of acid and base functional groups that could be related to the catalyst consumption during reaction (400°C and oxidizing gases). It could also be related to alumina that is reported to have comparatively less acid and base groups [88].

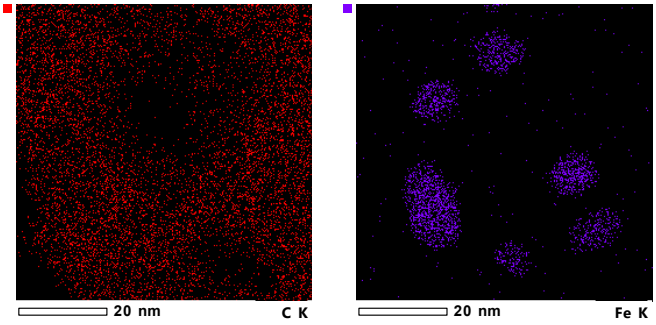

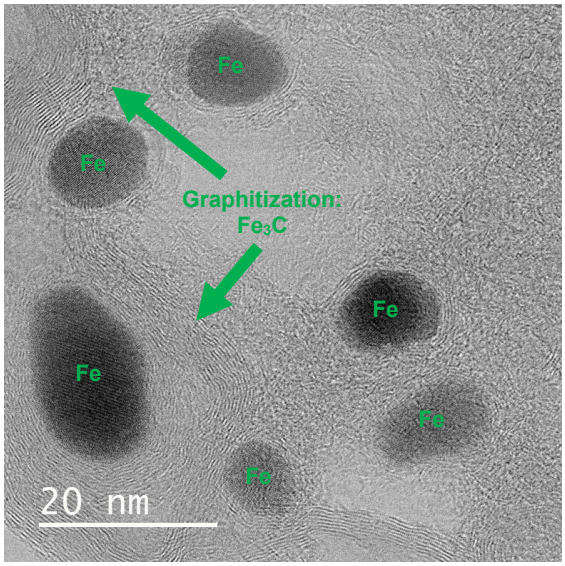

Figure 14. HRTEM images of fern biocarbon impregnated with Fe before pyrolysis (FFe-B) after RWGS

Conclusion

Biocarbon catalysts from fern and willow were produced, characterized and tested for RWGS reaction at 400°C and a ratio H_2/CO_2 of 3. This reaction consuming CO_2 could partake in FTS, effectively lowering both the H_2/CO ratio and the efficiency in the production of synthetic fuels. RWGS has attracted much attention as a potential means to widespread utilization of CO_2 through the production of syngas. The catalysts were tested in a fixed-bed reactor at a high temperature (400°C) considering the use in FTS. These catalysts exhibited a strong ability to retain significant amounts of Fe and Ni after the impregnation process, while they

also contain additional inherent metals. As a result, the synergistic effect of these metals could enhance the electronic properties of the active sites and facilitate the adsorption and dissociation of CO_2 and H_2. The combination of these properties allowed fern to outperform willow-based biocarbon catalysts in RWGS. The surface functional groups and metals such as AAEM in addition to Fe or Ni have resulted in O vacancies after reduction that could increase catalytic performance due to better CO_2 adsorption and activation. Depending on the impregnation, the introduction of metals on the structure of the biocarbon could affect availability and activity of these sites by blocking access or by creating additional sites for better electron exchange. This could result in catalysts with high performances, such as FNi-A, FFe-B and FNiFe. Moreover, the biocarbon catalysts exhibited promising stability in the reaction conditions by maintaining conversion and selectivity for at least 72h, while rust (Fe_2O_3) suffered severe C fouling. Complementary analytical techniques could contribute in elucidating the role and influence of the structure and metal bonding of biocarbon catalysts in the high activity observed. This could be achieved by the modification of the catalyst structure through changing the operating conditions such as pre-reduction but also by activating and stabilizing the biocarbon through high temperature H_2O activation. This would allow using the catalysts at higher temperatures, favoring RWGS while maintaining high selectivity. Additionally, future work should test catalysts performance in downstream reactions such as biofuel production by RWGS-assisted Fischer-Tropsch synthesis, CAMERE methanol synthesis, biogas reforming or conversion of pollutants in gaseous effluents. Finally, testing various inherently metal-rich biocarbon catalysts could help elucidate their high potential for RWGS.

Experimental Section

Induced coupled plasma – optic emission spectroscopy (ICP-OES)

100 ± 10 mg of biocarbon is weighed and inserted in Teflon tubes. This is repeated thrice (average RSD < 10%). Then, acid is added using a plastic graduated pipette to the 3 samples: 1.5 mL of H_2O_2, 4 ml of HNO_3 and 0.5 mL of HF. The Teflon tubes are inserted in enclosed iron reactors. The samples are then heated in a Berghof DAB reactor to 220°C for 8 hours to ensure total mineralization of the sample. In case of non-mineralization of the sample, extra acid is added and the sample is heated longer. After mineralization, the liquid samples are diluted to 50mL using distilled water. Using values of mass and volume, the sensitivity is at most 1 µg/g. The samples are then analyzed by ICP-OES based on standard samples of known concentration.

High resolution transmission electron microscopy (HRTEM)

The equipment is a JEOL JEM-ARM200F Cold FEG probe Cs corrected coupled with EDS/EELS for better determination of the chemical nature of the structure.

X-ray diffraction (XRD)

XRD is performed by the Philips PANalytical X'PERT PRO MDP diffractometer. The software used to extract data from the diffractogram is the PANalytical HighScore Plus. To identify the crystalline phases, the Crystallographic Open Database (COD) is used. 2θ spans 10 to 80° with a pace of 0.033°.

Temperature programmed desorption, oxidation and reduction (TPX)

Temperature Programed (TPX) Desorption (X = D), Oxidation (X = O) and Reduction (X = R) are used to characterize the density and binding force of acid, basic and reduction sites respectively. A gas (NH_3, CO_2 or H_2 respectively) is adsorbed at a low temperature and then they are desorbed as temperature increases, forming a peak. The position and surface area of the peaks indicate the strength and quantity of the sites. The device used is the Micromeritics Autochem 2920. The sample is first cleared under a flow of inert gas (He) at 40°C for 10 min followed by an isotherm at 110°C for 2h. Then, it is brought back to 50°C where the solid is then saturated with probe gases NH_3, CO_2, H_2 or He for 60 min then He is introduced for 2h. Probe gases are injected at a ratio with He of 5 %vol. µGC begins at this point and He continues to be injected at 50°C for 10 min before undergoing a programmed temperature rise to desorb the probe molecules. Temperature rises to 950°C and then is maintained for 2h. Desorption peaks are recorded during this program. This protocol is similar for TPR but adjustments are made to the heating ramps and duration of isotherms.

Specific surface area determination using Brunauer-Emmett-Teller (BET)

The device used is the Tristar II 3020. The analysis technique is based on the physisorption of gases at low temperatures. Before analyzing, the sample is dried, weighed and rid of gases from ambient and experimental atmosphere by heating at 110°C and vacuuming the sample to less than 100 mTorr, during 24h. To minimize interaction of He with the biocarbon surface, free space was calculated according to Micromeritics application notes 104 and 105. Samples at a room temperature of 293K were then submerged in a liquid N_2 bath at 77K. The isotherm was performed from relative pressures 0.025 to 0.993 and 0.993 to 0.427 for adsorption and desorption respectively. BET model was applied to at least 3 points under 0.3 relative pressure. The BET constant was positive and the correlation coefficient was superior to 0.999. The biocarbon were studied in triplicates as to guarantee repeatability of results. For the spent catalysts, the device used is a Micromeritics 3Flex and similar conditions were applied. The only difference is a 10h degassing.

Acknowledgements

The authors sincerely acknowledge the support provided by Eizhy, which provided shrubland biomass used in this study, as well as the European Union's Horizon 2020 research and innovation program under grant agreement No 637020−MOBILE FLIP for the willow biomass used in this study.

Keywords: Biocarbon • Catalyst • Iron • Nickel • Reverse water-gas shift mechanism

[1] U. Nations, “The Paris Agreement,” can be found under https://www.un.org/en/climatechange/paris-agreement.
[2] “CO2 Emissions in 2022 – Analysis,” can be found under https://www.iea.org/reports/co2-emissions-in-2022.
[3] “In focus: Reducing the EU’s dependence on imported fossil fuels,” can be found under https://commission.europa.eu/news/focus-reducing-eus-dependence-imported-fossil-fuels-2022-04-20_en.
[4] "AR6 Synthesis Report: Climate Change 2023 — IPCC" can be found under https://www.ipcc.ch/report/sixth-assessment-report-cycle/
[5] A. C. Ghogia, B. F. Machado, S. Cayez, A. Nzihou, P. Serp, K. Soulantica, D. Pham Minh, J. Catal. 2021, 397, 156–171.
[6] R. Munirathinam, D. Pham Minh, A. Nzihou, Ind. Eng. Chem. Res. 2018, 57, 16137–16161.
[7] M. Martinelli, M. K. Gnanamani, S. LeViness, G. Jacobs, W. D. Shafer, Appl. Catal., A, 2020, 608, 117740.
[8] L. M. Romero Millán, F. E. Sierra Vargas, A. Nzihou, Fuel 2020, 119527.
[9] L. Yang, CO2 Conversion via Reverse Water-Gas Shift Using Multicomponent Catalysts - University of Surrey, University of Surrey, 2021.
[10] J. A. Loiland, M. J. Wulfers, N. S. Marinkovic, R. F. Lobo, Catal. Sci. Technol. 2016, 6, 5267–5279.
[11] Q. Zhang, L. Pastor-Pérez, Q. Wang, T. Ramirez Reina, J. Energy Chem. 2022, 66, 635–646.
[12] L. Yang, L. Pastor-Pérez, J. J. Villora-Pico, A. Sepúlveda-Escribano, F. Tian, M. Zhu, Y.-F. Han, T. Ramirez Reina, ACS Sustainable Chem. Eng. 2021, 9, 12155–12166.
[13] Z. Zhang, G. Huang, X. Tang, H. Yin, J. Kang, Q. Zhang, Y. Wang, Fuel 2022, 309, 122105.
[14] P. S. Sai Prasad, J. W. Bae, K.-W. Jun, K.-W. Lee, Catal Surv Asia 2008, 12, 170–183.
[15] A. G. Kharaji, A. Shariati, M. A. Takassi, Chin. J. Chem. Eng. 2013, 21, 1007–1014.
[16] C.-Y. Chou, J. A. Loiland, R. F. Lobo, Catalysts 2019, 9, 773.
[17] E. Pahija, C. Panaritis, S. Gusarov, J. Shadbahr, F. Bensebaa, G. Patience, D. C. Boffito, ACS Catal. 2022, 12, 6887–6905.
[18] W. Benzinger, E. Daymo, M. Hettel, L. Maier, C. Antinori, P. Pfeifer, O. Deutschmann, Chem. Eng. J. 2019, 362, 430–441.
[19] F. Sun, C. Yan, Z. Wang, C. Guo, S. Huang, Int. J. Hydrogen Energy 2015, 40, 15985–15993.
[20] L. Deng, X. Ai, F. Xie, G. Zhou, Chem. - Asian J. 2021, 16, 949–958.
[21] C. Di Stasi, S. Renda, G. Greco, B. González, V. Palma, J. J. Manyà, Sustainability 2021, 13, 8939.
[22] J. L. Santos, L. F. Bobadilla, M. A. Centeno, J. A. Odriozola, C 2018, 4, 47.
[23] Y. Wang, Y. Shao, L. Zhang, S. Zhang, Y. Wang, J. Xiang, S. Hu, G. Hu, X. Hu, Fuel 2021, 293, 120426.
[24] X. Wang, Y. Liu, L. Zhu, Y. Li, K. Wang, K. Qiu, N. Tippayawong, P. Aggarangsi, P. Reubroycharoen, S. Wang, J. CO2 Util. 2019, 34, 733–741.
[25] A. Zakharova, M. W. Iqbal, E. Madadian, D. S. A. Simakov, ACS Appl. Mater. Interfaces 2022, 14, 22082–22094.
[26] Z. Zhao, M. Wang, P. Ma, Y. Zheng, J. Chen, H. Li, X. Zhang, K. Zheng, Q. Kuang, Z.-X. Xie, Appl. Catal., B, 2021, 291, 120101.
[27] L. F. Bobadilla, J. L. Santos, S. Ivanova, J. A. Odriozola, A. Urakawa, ACS Catal. 2018, 8, 7455–7467.
[28] G. W. Bruemmer, J. Gerth, U. Herms, Zeitschrift für Pflanzenernährung und Bodenkunde 1986, 149, 382–398.
[29] M. B. Rivera, M. I. Giráldez, J. C. Fernández-Caliani, Sci. Total Environ. 2016, 560–561, 254–265.
[30] K. S. Egorova, V. P. Ananikov, Organometallics 2017, 36, 4071–4090.
[31] M. Lambert, B. A. Leven, R. M. Green, ENVIRONMENTAL SCIENCE AND TECHNOLOGY BRIEFS FOR CITIZENS, 3.
[32] M. Said, L. Cassayre, J.-L. Dirion, X. Joulia, A. Nzihou, Waste Biomass Valorization 2017, 8, 2843–2852.
[33] W. Dastyar, A. Raheem, J. He, M. Zhao, Chem. Eng. J. 2019, 358, 759–785.
[34] J. Lee, K.-H. Kim, E. E. Kwon, Renewable Sustainable Energy Rev. 2017, 77, 70–79.
[35] L. Devi, K. J. Ptasinski, F. J. J. G. Janssen, Biomass Bioenergy 2003, 24, 125–140.
[36] S. Nanda, A. K. Dalai, F. Berruti, J. A. Kozinski, Waste Biomass Valorization 2016, 7, 201–235.
[37] H. C. Butterman, M. J. Castaldi, Environ. Sci. Technol. 2009, 43, 9030–9037.
[38] C. Guizani, M. Jeguirim, R. Gadiou, F. J. Escudero Sanz, S. Salvador, Energy 2016, 112, 133–145.
[39] M. Sekar, V. K. Ponnusamy, A. Pugazhendhi, S. Nižetić, T. R. Praveenkumar, J. Environ. Manage. 2022, 302, 114046.
[40] Y. Chai, M. Bai, A. Chen, L. Peng, J. Shao, C. Shang, C. Peng, J. Zhang, Y. Zhou, Sci. Total Environ. 2022, 822, 153426.
[41] J. S. Lee, H. S. Kim, N.-K. Park, T. J. Lee, M. Kang, Chem. Eng. J. 2013, 230, 351–360.
[42] B. S. R. J, M. Loganathan, M. S. Shantha, Int. J. Chem. React. Eng. 2010, 8, DOI 10.2202/1542-6580.2238.
[43] Z. S. Fishman, Y. He, K. R. Yang, A. W. Lounsbury, J. Zhu, T. M. Tran, J. B. Zimmerman, V. S. Batista, L. D. Pfefferle, Nanoscale 2017, 9, 12984–12995.
[44] X. Su, X. Yang, B. Zhao, Y. Huang, J. Energy Chem. 2017, 26, 854–867.
[45] P. Kaiser, R. B. Unde, C. Kern, A. Jess, Chem. Ing. Tech. 2013, 85, 489–499.
[46] Y. A. Daza, J. N. Kuhn, RSC Adv. 2016, 6, 49675–49691.
[47] N. T. Mai, N. H. Nguyen, T. Tsubota, Y. Shinogi, S. Dultz, M. N. Nguyen, Colloids Surf., A, 2019, 583, 123937.
[48] J. Hyväluoma, M. Hannula, K. Arstila, H. Wang, S. Kulju, K. Rasa, J. Anal. Appl. Pyrolysis 2018, 134, 446–453.
[49] M. González Martínez, C. Dupont, D. da Silva Perez, L. Míguez-Rodríguez, M. Grateau, S. Thiéry, T. Tamminen, X.-M. Meyer, C. Gourdon, J. Environ. Manage. 2019, 236, 551–560.
[50] T. K. Trinh, T. Tsubota, S. Takahashi, N. T. Mai, M. N. Nguyen, N. H. Nguyen, Sci Rep 2020, 10, 19974.
[51] A. Siatecka, K. Różyło, Y. S. Ok, P. Oleszczuk, Sci. Total Environ. 2021, 789, 147458.
[52] S. V. Vassilev, D. Baxter, L. K. Andersen, C. G. Vassileva, T. J. Morgan, Fuel 2012, 94, 1–33.
[53] F. J. Zhaol, S. J. Dunham, S. P. McGrath, The New Phytologist 2002, 156, 27–31.
[54] G. Akomolafe, Dedeke, S. S.A, 2013.
[55] C. Keller, C. Ludwig, F. Davoli, J. Wochele, Environ. Sci. Technol. 2005, 39, 3359–3367.
[56] J. Korzeniowska, E. Stanislawska-Glubiak, Int. J. Environ. Sci. Technol. 2019, 16, 1999–2008.
[57] E. Meers, B. Vandecasteele, A. Ruttens, J. Vangronsveld, F. M. G. Tack, Environ. Exp. Bot. 2007, 60, 57–68.
[58] K. A. Wani, Z. M. Sofi, J. A. Malik, J. A. Wani, in Bioremediation and Biotechnology, Vol 2: Degradation of Pesticides and Heavy Metals (Eds.: R.A. Bhat, K.R. Hakeem, M.A. Dervash), Springer International Publishing, Cham, 2020, pp. 161–174.
[59] R. Reeves, “A global database for plants that hyperaccumulate metal and metalloid trace elements - New Phytologist” can be found under https://nph.onlinelibrary.wiley.com/doi/full/10.1111/nph.14907.
[60] X. Chen, Y. Chen, C. Song, P. Ji, N. Wang, W. Wang, L. Cui, Front. Chem. 2020, 8.
[61] H. T. Luk, C. Mondelli, S. Mitchell, S. Siol, J. A. Stewart, D. Curulla Ferré, J. Pérez-Ramírez, ACS Catal. 2018, 8, 9604–9618.

[62] J. Xu, X. Gong, R. Hu, Z. Liu, Z. Liu, Mol. Catal. 2021, 516, 111954.
[63] X. Yang, X. Su, X. Chen, H. Duan, B. Liang, Q. Liu, X. Liu, Y. Ren, Y. Huang, T. Zhang, Appl. Catal., B, 2017, 216, 95–105.
[64] T. Béguerie, E. Weiss-Hortala, A. Nzihou, Sci Rep 2022, 12, 21492.
[65] A. C. Ghogia, L. M. Romero Millán, C. E. White, A. Nzihou, ChemSusChem 2023, 16, e202201864.
[66] N. Guskos, E. A. Anagnostakis, V. Likodimos, T. Bodziony, J. Typek, M. Maryniak, U. Narkiewicz, I. Kucharewicz, S. Waplak, J. Appl. Phys. 2004, 97, 024304.
[67] J. Xiong, J. Xu, M. Zhou, W. Zhao, C. Chen, M. Wang, W. Tan, L. Koopal, ACS Sustainable Chem. Eng. 2021, 9, 2600–2608.
[68] A. C. Ghogia, “Développement de catalyseurs monolithiques structurés du type Co/C/mousse pour le procédé de synthèse Fischer-Tropsch,” can be found under http://www.theses.fr/s184711.
[69] M. Ducousso, "Gasification biochar reactivity toward methane cracking" can be found under https://www.theses.fr/2015EMAC0016.
[70] S. V. Vassilev, D. Baxter, L. K. Andersen, C. G. Vassileva, Fuel 2010, 89, 913–933.
[71] S. Xia, K. Li, H. Xiao, N. Cai, Z. Dong, C. xu, Y. Chen, H. Yang, X. Tu, H. Chen, Bioresour. Technol. 2019, 287, 121444.
[72] M. M. Yung, A. K. Starace, C. Mukarakate, A. M. Crow, M. A. Leshnov, K. A. Magrini, Energy Fuels 2016, 30, 5259–5268.
[73] J. Zhang, Y. Yang, J. Liu, B. Xiong, Appl. Surf. Sci. 2021, 558, 149866.
[74] L. Wang, H. Liu, Y. Liu, Y. Chen, S. Yang, J. Rare Earths 2013, 31, 559–564.
[75] P. Tarifa, M. González-Castaño, F. Cazaña, A. Monzón, H. Arellano-García, Fuel 2022, 319, 123707.
[76] L. M. R. Millan, "Steam gasification of tropical lignocellulosic agrowaste : impact of biomass characteristics on the gaseous and solid by-products" can be found under https://www.theses.fr/2018EMAC0011.
[77] M. Ducousso, Gasification Biochar Reactivity toward Methane Cracking.
[78] M. Hervy, “Valorisation de Chars Issus de Pyrogazéification de Biomasse Pour La Purification de Syngas : Lien Entre Propriétés Physico-Chimiques, Procédé de Fonctionnalisation et Efficacité Du Traitement” can be found under https://www.theses.fr/2016EMAC0013.
[79] E. G. Gioria, “Colloidal nanoparticles for the rational design of (multi) metallic heterogeneous catalysts” can be found under https://depositonce.tu-berlin.de/items/b0ccbc99-8b7b-40dc-9533-a94ccd76d1a2.
[80] Z. Chen, L. Liang, H. Yuan, H. Liu, P. Wu, M. Fu, J. Wu, P. Chen, Y. Qiu, D. Ye, L. Chen, Appl. Catal., B, 2021, 298, 120507.
[81] Y. Liu, P. R. Murthy, X. Zhang, H. Wang, C. Shi, New J. Chem. 2021, 45, 22444–22449.
[82] S.-C. Lee, J.-S. Kim, W. C. Shin, M.-J. Choi, S.-J. Choung, J. Mol. Catal. A: Chem. 2009, 301, 98–105.
[83] M. C. Le, K. L. Van, T. H. T. Nguyen, N. H. Nguyen, J. Chem. 2017, 2017, e4361056.
[84] K. Feng, J. Tian, M. Guo, Y. Wang, S. Wang, Z. Wu, J. Zhang, L. He, B. Yan, Appl. Catal., B, 2021, 292, 120191.
[85] E. Gioria, P. Ingale, F. Pohl, R. N. d’Alnoncourt, A. Thomas, F. Rosowski, Catal. Sci. Technol. 2022, 12, 474–487.
[86] Z. Gao, Y. Meng, H. Shen, B. Xie, Z. Ni, S. Xia, Mol. Catal. 2021, 516, 111992.
[87] J. A. Hernandez Lalinde, P. Roongruangsree, J. Ilsemann, M. Bäumer, J. Kopyscinski, Chem. Eng. J. 2020, 390, 124629.
[88] L. G. T. Gouveia, C. B. Agustini, O. W. Perez-Lopez, M. Gutterres, J. Environ. Chem. Eng. 2020, 8, 103823.

Entry for the Table of Contents

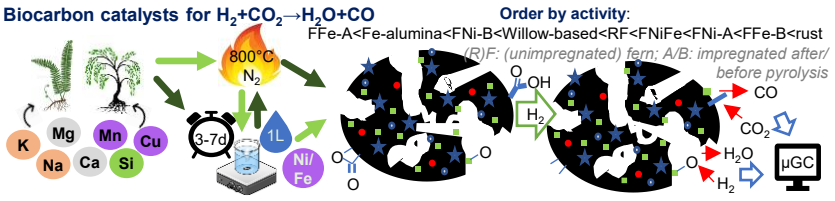

Biocarbon catalysts were prepared from iron and nickel impregnated pyrolyzed fern and willow to mimic plants issued from phytoremediation. Reverse water-gas shift (RWGS) catalyzed by these catalysts was studied at 400°C and H_2/CO_2=3 as RWGS can partake in Fischer-Tropsch synthesis to form synthetic fuel. They were highly selective (>84%) with fair conversion (<17%) and showed no long-use (288h) deactivation.